Correlation of the structures of dense silica with x-ray Raman spectra

Huiyao Kuang
Department of Physics and Engineering Physics, University of Saskatchewan, Saskatoon SK S7N 5E2, Canada

Christoph J. Sahle
ESRF, The European Synchrotron, 71 Avenue des Martyrs, CS40220, 38043 Grenoble Cedex 9, France

Sylvain Petitgirard
Department of Earth Sciences, Institute of Geochemistry and Petrology, ETH, 8092 Zurich, Switzerland

John S. Tse*
Department of Physics and Engineering Physics, University of Saskatchewan, Saskatoon SK S7N 5E2, Canada

(Received 28 July 2023; revised 27 November 2023; accepted 22 January 2024; published 16 February 2024)

The structure of mineral glasses at high pressure is often used as a model to understand corresponding melts. In this regard, silica, a prototypical oxide glass, has been studied extensively by theoretical simulations and experiments. A recent study of the oxygen K-edge x-ray Raman scattering (XRS) spectra of SiO_2 glass suggested a relationship between energies at the centers of gravity of the XRS spectra with the bulk density and electronic density of states at Mbar pressure. It was further proposed that the oxygen atoms are 4-coordinated to silicon, so-called quadclusters, at pressures above 1 Mbar. Here, we investigate the theoretical basis of this empirical observation from the simulation of the XRS spectra and analysis of the structure and bonding of a silica glass up to 2 Mbar. The theoretical results reproduce the observed x-ray absorption spectra, and the relationship between the center of gravity of the O K-edge absorption with pressure. However, we show that the trend is not due to the proposed occurrence of oxygen quadclusters. It is simply a compaction effect and there are no characteristic spectral features that can be attributed to the additional oxygen-silicon coordination.

DOI: 10.1103/PhysRevB.109.054110

I. INTRODUCTION

Silica (SiO_2) is one of the most abundant materials on Earth. The amorphous form, SiO_2 glass, is a prototypical example of amorphous oxides and other Si-containing mineral glasses and melts in the deep Earth [1,2]. Over the years, the structure of SiO_2 glass at high pressure has been extensively studied by experiments and computer simulations [1–9]. At ambient conditions, all Si atoms in SiO_2 glass are 4-coordinated to the nearest O atoms. Furthermore, O atoms are 2-coordinated to neighboring Si atoms and form the corner-sharing Si-O_4 silica moieties. 5-coordinated Si-O_5 was proposed to exist from x-ray diffraction data at 27 GPa [10]. However, the debate of whether the Si atoms were 5-coordinated or a mixture of 4- and 6-coordinated is still unsettled [11,12]. First-principles molecular dynamics (FPMD) calculations also proposed the existence of 5-coordinated Si earlier [13]. FPMD calculations across a broader pressure range reported that the 5-coordinated Si starts to appear at 12 GPa along with the 6-coordinated Si at the expense of 4-coordinated Si, whose proportion drops to 0 above 64 GPa [5]. The fraction of the 5-coordinated Si starts to decrease after 60 GPa, while 6-coordinated Si continues to increase and becomes the dominant species [5]. The theoretically predicted changes in the Si-O coordination number is in close agreement with the analysis from *in situ* high-pressure neutron diffraction in the pressure range from 0 to 17.5 GPa [14]. Upon further compression to 100 GPa, the theoretical calculation [5] suggested the formation of 7-coordinated Si above 100 GPa was supported by an anomaly in the bulk sound velocity observed in *ab initio* simulations and experiment [1,7]. Recently, direct measurement of refractive index up to 145 GPa was reported to verify the SiO_2 glass structure, and the results are in good agreement with previous studies [8]. Although numerous research has been performed to understand SiO_2 glass, a few questions and misunderstandings about the densification mechanisms still exist.

Recently, SiO_2 glass was studied up to 160 GPa using O K-edge x-ray Raman scattering (XRS) spectroscopy [15]. Analysis of the results presented an empirical relationship between the position of the center of gravity (E_C) of the excitation band with pressure. It was also shown that a linear relationship can be established between the O-O distances and the density of the glass with E_C. Furthermore, the authors suggest that the O atoms in the SiO_2 glass will become coordinated with four closest Si forming O-Si quadclusters at 160 GPa [15]. This assignment is based on the apparent observation of a feature in the XRS spectra at about 548 eV energy loss, which increases with pressure. This feature is interpreted as a signature of

*john.tse@usask.ca

 ©2024 American Physical Society

the transformation of 3-coordinated O to 4-coordinated O by formation of oxygen quadclusters. No theoretical explanation was offered to rationalize the empirical relationships. In view of the limited resolution and statistical accuracy of the XRS spectra, confirmation of the existence of O-Si_4 quadclusters in SiO_2 glass requires further investigation.

In high-pressure silica, Si-O bonds are formed by the interaction between hybridized valence $3s$, $3p$, and $3d$ orbitals of Si with the O $2s$ and $2p$ orbitals. Since O does not possess low-lying empty d orbitals to expand the coordination, the formation of quadclusters with Si is unusual. Coordination is not bonding. Coordination simply measures the number of nearest-neighbor atoms. Bonding involves chemical interactions due to the sharing of electrons between two adjacent atoms forming a chemical bond. If there was a 4-coordinated O-Si bond, most likely the electrons from the O lone pair are donated to the d orbitals of Si, i.e., the sharing of electrons. In a formal chemistry language, this should be referred as a "dative" bond, i.e., a covalent bond (a shared pair of electrons) in which both electrons come from the same atom. A previous FPMD calculation of SiO_2 glass simulated the structures up to 198 GPa and successfully reproduced the experimental diffraction patterns, the equation of states (EOS), O K-edge XRS spectra, and the velocity of sound [5]. A recent experimental study on the Si $L_{2,3}$ and O K edge up to 108 GPa also found good agreement between the measured spectra and those calculated based on the simulated FPMD structures including core-valence electron correlation effects [2]. In this study, we extend the XRS spectra calculations to 198 GPa and compare with the recent experiment to investigate whether oxygen quadclusters can indeed exist in glassy SiO_2 and to shed light on the fundamental physics behind the suggested empirical correlations of the excitation energy with the physical property of this ubiquitous glass.

II. METHODS

The amorphous SiO_2 model is composed of 24 SiO_2 units (72 atoms in total). Randomly chosen snapshots were taken from trajectories obtained for pressures of 110, 126, 134, 142, 150, 166, 174, 182, and 198 GPa in the previous FPMD simulations [5]. At each pressure, the O K-edge XAS and XRS were calculated using the OCEANcode [16,17] from the average of four snapshots chosen randomly from the MD trajectory. At each pressure, XRS spectra at both low-momentum ($q = 2.5$ Å) and high-momentum ($q = 6.5$ Å) transfer were computed. Each computed spectrum represents an average over all O (48) atoms and an angular average over 18 uniformly chosen momentum transfer directions. Local density approximation (LDA) norm-conserving pseudopotentials using Troullier-Martins method were used in the OCEAN calculation. Valence configuration of O is $2s^2 2p^4$, and Si is $3s^2 3p^2$. The ground-state charge density and the Kohn-Sham orbitals were obtained from a self-consistent field (SCF) density functional theory (DFT) calculation employing the local density approximation to the exchange-correlation functional with the QUANTUM ESPRESSO code [18,19]. The plane waves were truncated at 60 Ryd. A $2\times2\times2$ k-point grid was used. Screening of the core hole was computed within the random phase approximation (RPA) including 1200 bands in the final state within a cutoff radius of 5 bohrs around each oxygen atom. Then the Bethe-Salpeter equations (BSE) [20] are solved to compute the XRS spectra convoluted with a Lorentzian broadening of width 0.4 eV. A $3\times3\times3$ k-point set was used in the screening and BSE calculations. The x-ray absorption spectra (XAS) were calculated in a similar manner but assuming dipole excitation rules. In this case, the average of spectra calculated with the x-ray polarization vector along the three principal axes was used. The final spectra were aligned along the energy-loss axis with the onset of the experimental spectra of Lee *et al.* [15]. The VASP (Vienna *ab initio* simulation package) code was used to calculate the electronic properties, which used a cutoff energy of 530 eV. The CRITIC2 code [21,22], which uses Bader's quantum theory of atoms in molecules (QTAIM) [23–26] to search for the relevant critical points, was utilized to characterize the chemical bonds. Four randomly chosen structures from the FPMD trajectory at 198 GPa were used.

III. RESULTS AND DISCUSSION

A. Coordination number and bond angles

First, we compare the structures of amorphous SiO_2 from FPMD simulations with those derived from diffraction experiments to validate whether the theoretical structures are reasonable. Since the structural evolution and O K-edge XRS spectra below 110 GPa have been evaluated already and have been found to compare well with experiment [2], here, we only focus on the results above 110 GPa. The relative percentage changes of the O-Si and Si-O coordination numbers with pressure are plotted in Figs. 1(a) and 1(b), respectively. The cutoff radius was chosen as 1.9 Å, which is between the covalent distance of 1.77 Å and the first minimum in the RDF at 2.2 Å (the O-Si and O-O radial distribution functions are compared in the Supplemental Material [27]).

Overall, the percentage of the O-Si coordination number does not change significantly from 110 to 198 GPa. The 3-coordinated O dominates over the pressure range studied. The percentage of 3-coordinated O increases to 90% at 166 GPa, and then slightly decreases by about 7% from 166 to 198 GPa. The fraction of the 2-coordinated O is reduced from 15% to 10%. 4-coordinated O starts to appear at 134 GPa but the fraction is relatively small at about 2%. At 198 GPa, the percentage of the 4-coordinated O increases to 6%. The Si-O coordination number shows more subtle changes as shown in Fig. 1(b). We found no 4-coordinated Si in our system at the studied pressure range, in agreement with the previous study at lower pressures, which showed that the 4-coordinated Si has completely transformed to higher coordination above 65 GPa [5]. Above 50 GPa, the 6-coordinated Si accounted for more than 50% and continued to increase. 5-coordinated Si makes up about 45% and starts to exhibit a downward trend [5]. As it is shown in Fig. 1(b), the percentage of 5-coordinated Si decreases rapidly from 29% to 8% between 110 and 198 GPa. Within the same pressure range, the percentage of 6-coordinated Si increases from 71% to 88%. At 198 GPa, there is a slight increase in the fraction of the 7-coordinated Si to 4%. It is apparent that there is a concomitant

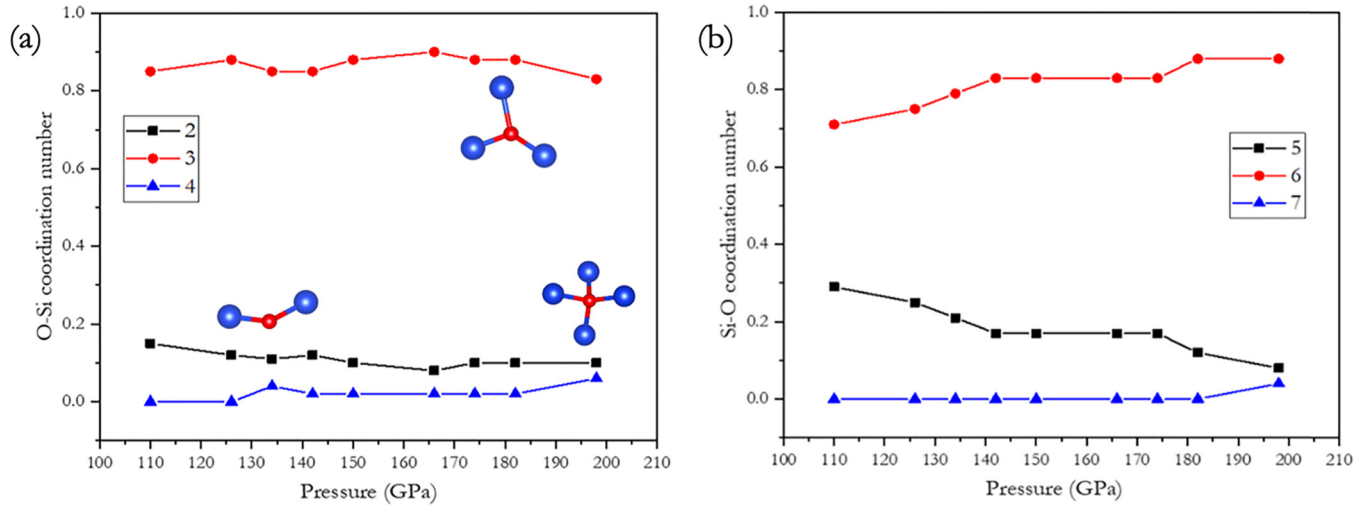

FIG. 1. The fraction of (a) O-Si and (b) Si-O coordination numbers from 110 to 198 GPa as extracted from the FPMD simulation snapshots. The cutoff distance was set to 1.9 Å, which is between the covalent distance of 1.77 Å and the first minimum of RDF of 2.2 Å.

change in the trend of the O-Si and Si-O coordination numbers close to 170 GPa. The observations indicate there may be changes in the local structure around the Si and O. The bond angle distribution plots of O-Si-O and Si-O-Si are shown in the Supplemental Material [27].

B. Oxygen *K*-edge spectra: Experiment versus theory

The simulated O *K*-edge XRS spectra from ambient pressure up to 108 GPa have already been found to agree very well with experiments (Fig. 1 in Ref. [2]). Here, we only discuss the structure of amorphous SiO_2 and compare our results with those reported in Lee *et al.* (Ref. [15]) at similar pressures. The experimental low-momentum transfer O *K*-edge spectra reported in Lee *et al.* (Ref. [15]) and Petitgirad *et al.* (Ref. [2]) at pressure higher than 100 GPa are compared with the calculations in Fig. 2.

The experimental spectra of Lee *et al.*, utilizing the lowest-energy resolution of 1.4 eV, are several hundreds of meV sharper than the calculated spectra. This raises questions about introducing additional polycapillary focusing optics inside a Johann spectrometer for the suppression of background scattering from the gasket material compared to software slitting as performed by Petitgirard *et al.* [28,29].

The simulated spectra are in overall agreement with the two experimental results. However, the calculated spectrum is clearly broader than the result of the high-resolution experiment by Petitgirard *et al.* This is possibly due to the relatively large full width at half-maximum of 0.4 eV used to broaden the calculated spectra. The calculations reproduce the two-peak pattern in the observed spectra with an energy difference of about 4 eV. At ambient pressure, the experimental results from Lee *et al.* only show one peak at 538 eV (Fig. 1 in Ref. [15]). This excitation persists with increasing pressure. However, a new peak at higher energy of approximately 543 eV starts to emerge from 24 GPa. Upon further pressure increase, both peaks shift to higher excitation energies and then merge into a broad band.

In comparison, the high-resolution result reported in Ref. [2] at 108 GPa shows only one peak at about 23 eV. In contrast, the spectra obtained by Lee's experiment at 100 GPa can be differentiated into two features at 20 and 24 eV, although the second feature is not as strong and appeared as a shoulder, keeping in mind that the statistical accuracy of the experimental results complicates definite feature recognition and assignment. In view of the instrumental resolution and the artificial broadening of the calculated spectra, overall, the simulated XRS spectra at low-momentum transfer are consistent with the experiments. The agreement supports that the predicted amorphous SiO_2 structures from MD simulations

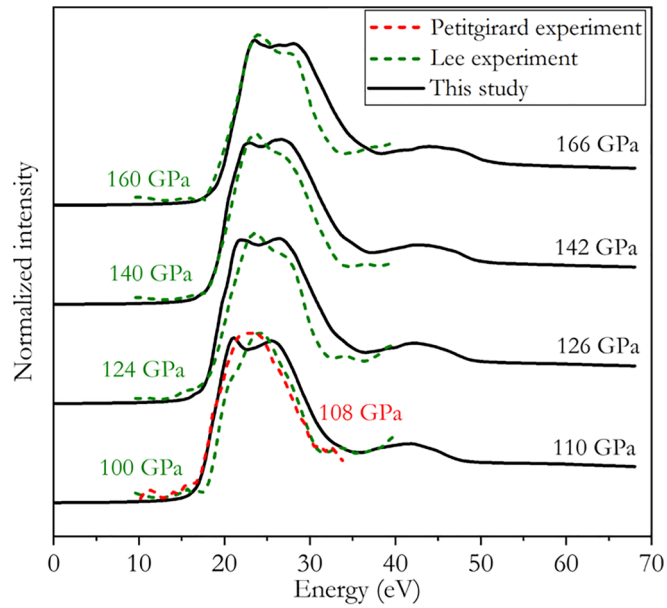

FIG. 2. Comparison of the simulated low-q XRS of O K edge with experimental results. The 110-GPa XRS is compared with Petitgirard's results at 108 GPa (blue dashed line) [2]. The XRS spectra at 126, 142, and 166 GPa are compared with Lee's experimental results at 124, 140, and 160 GPa, respectively (green dashed lines) [15].

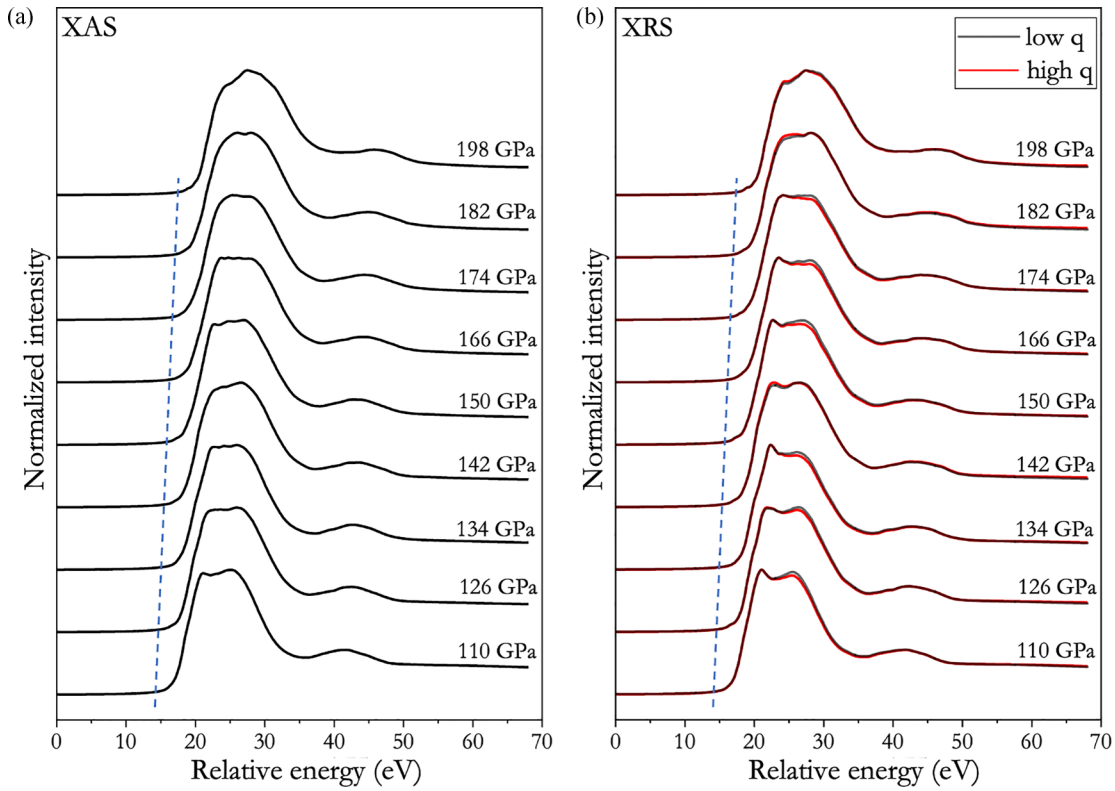

FIG. 3. The average O K-edge (a) XAS, (b) XRS at low-q and high-q spectra from 110 to 198 GPa obtained by calculation.

are reasonable, but casts some doubts about the detailed trends observable in experiments with low statistical accuracy and low-energy resolution.

C. Momentum transfer dependence

Figure 3 compares the computed O K-edge XAS and low- and high-momentum transfer XRS spectra for pressures between 110 and 198 GPa. The edge onset shifts gradually to higher energy as the pressure is increased. The XAS and low-q XRS spectra are almost identical [Figs. 3(a) and 3(b)]. The XAS and XRS patterns are similar in the low-q limit. At high-momentum transfer, the spectra differ only slightly from the low-q spectra, indicating the contribution of nondipolar excitations is small. The theoretical results are consistent with the XRS spectra measured at 0 and 108 GPa showing very little difference between the low- and high-q XRS spectra except the growing contribution of monopole transitions at the edge onset with increasing momentum transfer q (Fig. 4).

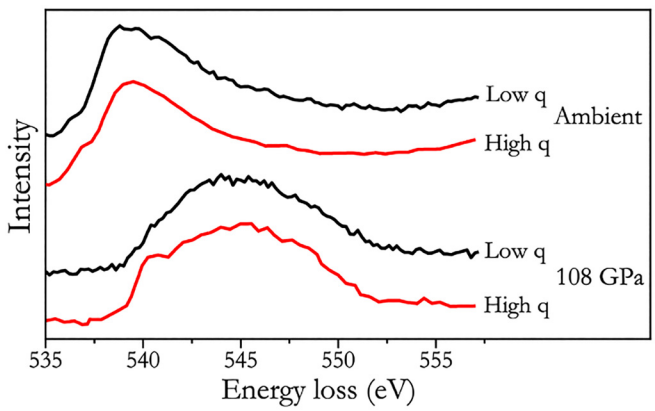

FIG. 4. XRS spectra measured at 0 and 108 GPa using low- and high-momentum transfer as taken from Ref. [2]. Low q: 2.5 Å^{-1}; high q: 6.5 Å^{-1}.

According to Ref. [5], the oxygen atoms are pushed towards the silicon's first-nearest-neighbor coordination shell upon compression. The change in the Si-O coordination is accompanied by the hybridization of the silicon valence 3s and 3p with the Si 3d orbitals, thus forming new excitation channels. The new interaction is exemplified by the occurrence of a second peak in the O K-edge XRS at higher excitation energy [5]. The new peak is clearly revealed in the O K-edge XRS spectrum of six-coordinated stishovite at 545 eV [2,15]. At low q, only dipolar transitions, i.e., $\Delta l = \pm 1$, dominate. So, the O 1s core electron is excited to empty states with p symmetry. At high q, nondipolar excitations, e.g., quadrupolar transitions with $\Delta l = \pm 2$ become accessible. However, Fig. 3 shows that the XRS spectra for low q and high q are almost identical, which indicates that the origin of the new peak cannot be quadrupolar excitations. The intensity of the low-q spectrum is slightly higher than at high q at the 24-eV peak. The discrepancy gradually narrows down with pressure. At 198 GPa, the low-q and high-q XRS spectra overlap. This indicates that d orbitals of O do not contribute to bonding in the amorphous SiO_2.

D. Center of gravity E_C

Following the method described in the Supplemental Material of Ref. [15], we calculated the center of gravity E_C of

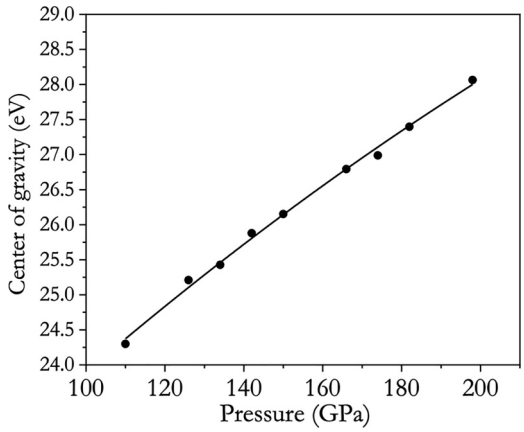

FIG. 5. Center of gravity E_C in the O K-edge low-q XRS spectra of SiO_2 glass versus pressure.

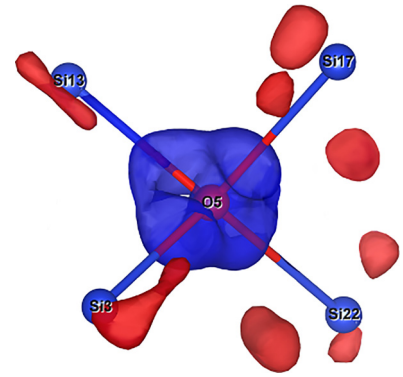

FIG. 6. The charge density difference plot. Red isosurfaces denote negative isovalues (electron deficit). Blue isosurfaces denote positive isovalues (electron surplus). The isovalues are 0.031 e/Å^3 (Si atoms are shown in blue, and the O atom in red).

the calculated XRS spectra at different pressures. In essence, a baseline was drawn from the onset of the first band to the minimum at about 35 eV. The region under the baseline was treated as background and we calculated the center of gravity for the resulting, background-subtracted, spectra. The results are plotted and fitted to a second-order polynomial curve in Fig. 5. With increasing pressure, E_C increases almost linearly. E_C is 24.3 eV at 110 GPa and increases to 28.1 eV at 198 GPa. The slope of the linear region from 100 to 160 GPa of Fig. 3(a) in Ref. [15] is 0.015 eV/GPa, while the slope from our calculation is 0.041 eV/GPa, which is about three times larger. Our results show the relationships obtained in Ref. [15] is qualitatively correct, however, its relation to the existence or nonexistence of 4-coordinated oxygen remains elusive. E_C of known crystalline phases with threefold oxygen coordination seem to correlate well with the findings for E_C of the compressed glass by Lee *et al.* (see Fig. 3 in Ref. [15]). The interpretation of E_C in terms of coordination further will have to encompass the spectral changes observable of the crystalline phases when subjected to pressure (i.e., the coordination number of the α-PbO_2 phase may remain constant up to its phase boundary, however, its E_C value shifts due to the compressed Si-O distance [30] rather than a change in coordination).

E. Oxygen quadclusters

To investigate whether O quadclusters can exist at high pressure, the trajectory at 198 GPa was inspected carefully. Three O-Si_4 (quad)clusters were found with a O-Si cutoff of 1.9 Å. It should be noted that even if the Si atoms are compressed towards the oxygen at high pressure increasing the nearest-neighbor coordination, it does not necessarily mean that they are covalently bonded to the central O atom. To analyze the interaction, we chose one of the O-Si_4 clusters for a further detailed analysis.

1. Electron density maps

To quantify the bonding of the O-Si_4 quadclusters, we investigated the electronic structures using different methods. First, we calculated the charge density difference between the superimposed atomic density and the charge density after the converged SCF calculation. The results are shown in Fig. 6 and provide information on the rearrangement of electrons in the O-Si_4 cluster. The red isosurfaces denote negative (electron deficit) in the region and the blue isosurfaces indicate positive isovalues (electron surplus). Figure 6 clearly shows the ionic nature of the Si interaction that electrons are transferred from the surrounding Si atoms to the O. Therefore, the formation of four O-Si "bonds" in amorphous SiO_2 seems possible. The charge transfer from O to Si is supported by the calculation of Bader volume and the according atomic charge density of the Si and O atoms. Results of this Bader analysis are shown in Figs. 7(a) and 7(b), respectively, as quantitative measurement of the change in the electron occupancy upon compression. The Bader volume of both Si and O decrease with increasing pressure, albeit a smaller reduction at the Si site is evident. The Bader volume of O decreases from about 8.5 to 7.5 Å^3 when the system is compressed from 110 to 198 GPa. In comparison, the Si atoms are less compressible with a smaller decrease from about 2.4 to 2.2 Å^3. It indicates that the compression of the amorphous SiO_2 is mainly due to the crowding of O atoms in the vicinity of Si, as the Si atoms are harder to compress in this pressure range. The distribution of the Si Bader volumes is very narrow at 110 GPa, only ranging from about 2.0 to 2.8 Å^3. The distribution becomes even narrower at 198 GPa. According to Fig. 1(b), the 6-coordinated Si atoms remain dominant at over 75% in this pressure range with a small increase in the proportion, which results in a narrower distribution of the Bader volumes. When compared to Fig. 1(a), the percentage of 3-coordinated O remains almost unchanged at above 80%. The volume distribution of the O atoms is much broader at 110 GPa, and 198 GPa of around 1.8 Å^3. This broad distribution is due to the simultaneous existence of oxygen with different nearest neighbors as the fraction of 2- and 3-coordinated oxygen does not show a significant change with increasing pressure. Figure 7(b) shows the charge density of Si and O atoms.

2. Density of states

We now turn our attention to the electronic structure. The projected density of states (pDOS) of O at the ground state SiO_2 at each pressure were calculated and are plotted in

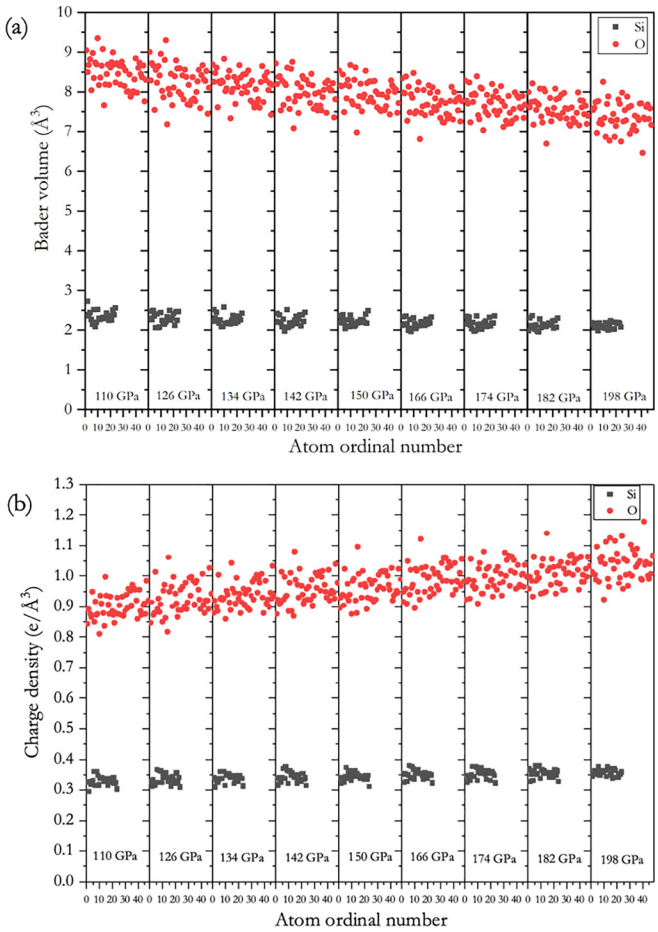

FIG. 7. Changes in the (a) Bader volume and (b) Bader charge density for Si and O as a function of pressure in the amorphous SiO_2 glass.

Fig. 8(a). The *s*, *p*, and *d* symmetries are shown in black, red, and blue, respectively. The Fermi level is aligned at 0 eV. The conduction band is from about 5 to 10 eV, which is dominated by the O *p* orbital. This agrees with Fig. 3(b), where very few O 1*s*-orbital electrons are excited to the empty orbitals with *d* symmetry. However, Fig. 8(a) also shows that *s* and *d* orbitals contribute to the conduction band. The density of states (DOS) of *s* and *d* orbitals of O are about half of the *p* component. Figure 8(b) shows the percentage of the *d* component to the total DOS integrated from 2.5 to 12 eV versus pressure. The percentage of the O *d* orbital can be fitted to a second-order polynomial function showing an increasing trend with pressure. The percentage increases from 16% at 110 GPa to 21.5% at 198 GPa. Nevertheless, there are no significant changes in the XAS, and low-*q* and high-*q* XRS [Fig. 3(b)], which indicates that *d* orbitals of O do not contribute to the bonding.

3. Local O-Si$_4$ structure

From Bader volume and Bader charge analyses (Fig. 7), we observed that the electron density at the site of the O atoms increases with pressure. In other words, more electrons are pushed towards the O atom with increasing pressure. This raises the question whether a higher electron density around the atom means the formation of a fourth O-Si bond. To answer this question, we calculated the electron localization function (ELF) and performed a QTAIM analysis. Before discussing the results of the ELF and QTAIM analyses, the local structures of O-Si_4 clusters will be investigated (see below).

It is well known that the coordination number around an atom depends on the choice of the cutoff radius. The percentage of the 4-coordinated O atoms versus the O-Si cutoff distance at different pressures is plotted in Fig. 9. When the cutoff distance is set to 1.8 Å, no 4-coordinated O is observed

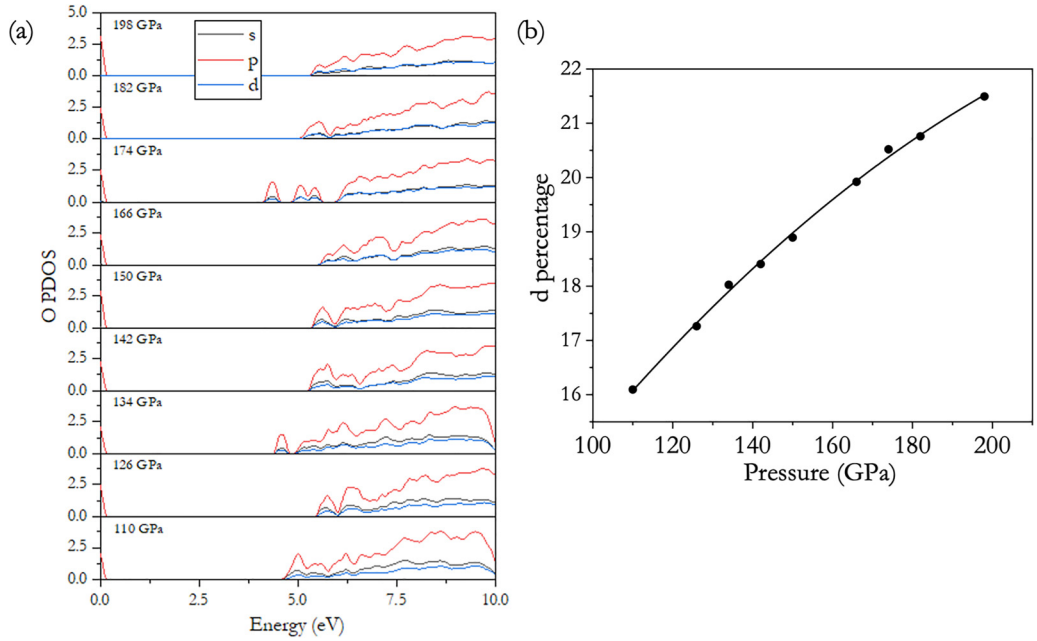

FIG. 8. (a) Projected density of states (pDOS) of O in amorphous SiO_2 calculated with PBE potential at different pressures. The DOS of the system was aligned to the Fermi level set at 0 eV. (b) The percentage of the *d* component to the total DOS integrated from 2.5 to 12 eV. The curve was fitted using the second-order polynomial function.

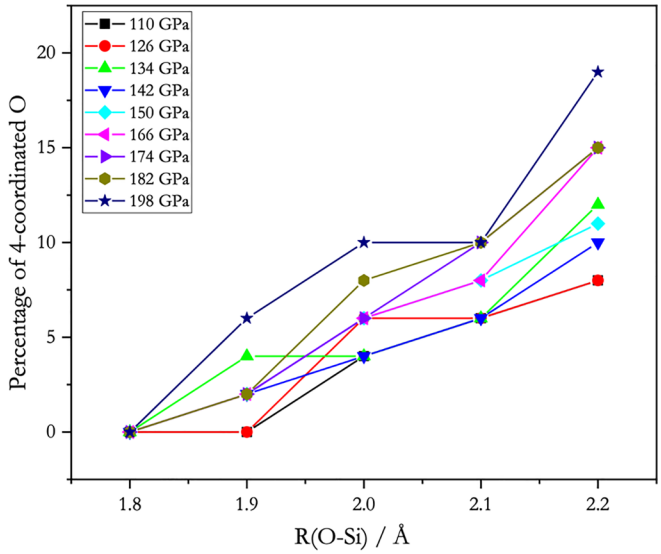

FIG. 9. The percentage of 4-coordinated O atoms versus the cutoff distance of the O-Si bond.

at all pressures up to 198 GPa. If we increase the cutoff distance to 1.9 Å, 4-coordinated O starts to appear above 134 GPa. The percentage of 4-coordinated O has a positive correlation with increasing O-Si cutoff distance. When the cutoff distance is increased to 2.2 Å, which is the first minimum of the RDF [Fig. 14(a)], amorphous SiO_2 shows a noticeable proportion of 4-coordinated O atoms at all pressures: at 110 GPa, about 7% of the O atoms are 4-coordinated and the fraction increases to about 18% at 198 GPa. We must be cautious that the choice of an unreasonably large cutoff distance can mistakenly overcount Si atoms that are not even close to the respective O. Inspection of the "quadclusters" found in the 198-GPa glass structure shows that there is always one O-Si bond that is longer than 1.8 Å in the 4-coordinated O atoms. Figure 9 also reveals the existence of long O-Si bonds in amorphous SiO_2. Since 4-coordinated O are not observed at all pressures when the cutoff radius is set to 1.8 Å and starts to appear only when using a larger cutoff radius, we can infer that the 4-coordinated O atoms have at least one O-Si bond that is longer than 1.8 Å. This is further exemplified in Fig. 10, where the local structures of

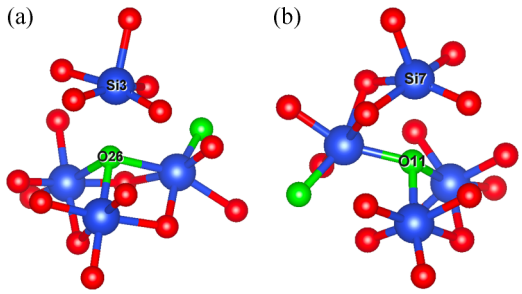

FIG. 10. Visualization of the local environment of "4-coordinated" oxygen atoms with cutoff radius 1.9 Å at (a) 110 GPa and (b) 198 GPa. The blue balls represent Si atoms, the red balls represent O atoms, and the green balls represent "4-coordinated" O atoms with cutoff radius of 2.2 Å.

4-coordinated O at 110 and 198 GPa are shown. In Figs. 10(a) and 10(b), the O atoms (O26 and O11) are both 3-coordinated if we use a cutoff distance of 1.8 Å. However, there are Si atoms (Si3 and Si7) nearby with a distance $<$2.2 Å, and thus they might be treated erroneously as a long O-Si bond, leading to the so-called 4-coordinated O atoms. For example, the O26-Si3 distance in Fig. 10(a) is 2.05 Å, and the O11-Si7 distance in Fig. 10(b) is 1.99 Å. The atoms are closer to each other due to the compression, but they do not form a fourth O-Si bond. This is because the lone pair electrons in the $2p$ orbitals of O hybridize with the Si $3d$ orbitals at high pressure forming a new excitation channel in the XRS spectra (as discussed in Sec. III C). Since Si has four valence electrons, the electrons involved in bonding are provided by O valence electrons. Given that there are only six valence electrons in O, each O atom can form at most three bonds with Si. Therefore, the 4-coordinated O cannot exist chemically.

4. Spectral fingerprints of quadclusters

To investigate the local structures of O atoms with different Si coordinations and to determine whether the XRS profile is sensitive to 4-coordinated O if it indeed exists in amorphous SiO_2, the XRS spectra at low momentum transfer of 2-, 3-, and 4-coordinated O atoms are compared at 110 and 198 GPa (Fig. 11). At 110 GPa [Fig. 11(a)], 2-coordinated O features a weak peak at about 18 eV, and several strong features from 20 to 25 eV. The spectrum of the 3-coordinated O atoms is very similar to the average spectrum in Fig. 3(b). It is because the 3-coordinated O atoms dominate at 110 GPa and 2-coordinated O only contribute a smaller fraction of 18%. The 3-coordinated O does not have the pre-edge feature. The first peak is found at about 20 eV, and a second peak at about 25 eV. The spectrum of the 4-coordinated O shows a small pre-edge feature at about 19 eV with broad and stronger peaks between 20 and 25 eV. At 198 GPa [Fig. 11(b)], the XRS spectra of the 2-, 3-, and 4-coordinated O are different from those at 110 GPa. The O-Si_2 coordinated atoms show a pre-edge feature at about 18 eV and, in addition, a broad shoulder develops at around 24 eV. A strong peak at about 32 eV can also be observed. The spectrum of the 3-coordinated O still highly resemble the average spectra shown in Fig. 3(b) since the 3-coordinated O atoms still make up more than 80% of all O. It shows a small peak at 24 eV, and a stronger peak at 28 eV. The 4-coordinated O spectrum has similar features at 24 and 28 eV, although the intensity of the first peak is stronger than the second one. It is clearly shown from Figs. 11(a) and 11(b) that the 2- and 3-coordinated O atoms in amorphous SiO_2 exhibit distinct XRS spectra because their local environments are different. However, in terms of the peak positions, no substantial differences are observed between the spectra of the 3- and 4-coordinated O atoms at both figures. The results suggest that the 3- and 4-coordinated O atoms do not have significant electronic differences in the local environment. Moreover, according to Fig. 1, the percentage of 4-coordinated O is only 6% at 198 GPa using a cutoff radius of 1.9 Å, i.e., only two or three O atoms are found to be 4-coordinated in the system. Thus, a small proportion of 4-coordinated O is not expected to alter the XRS spectral profile significantly.

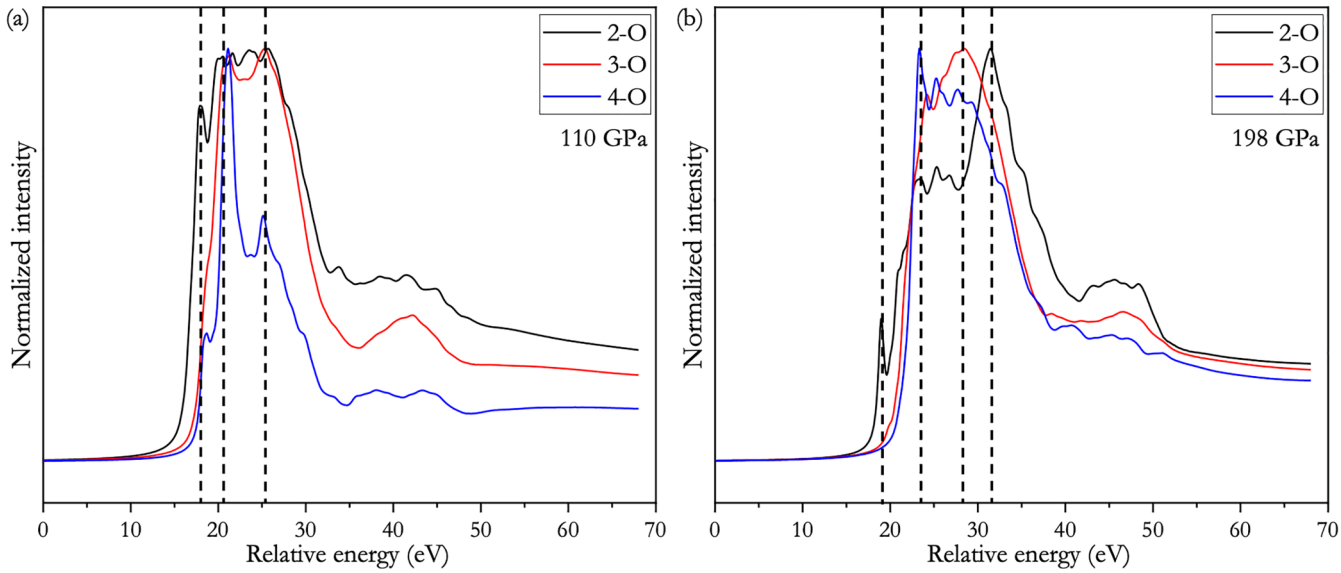

FIG. 11. The average O K-edge XRS spectra of the 2-, 3-, and 4-coordinated O atoms at (a) 110 GPa and (b) 198 GPa. The intensity was normalized to its maximum. The cutoff radius was set to be 2.2 Å. 4-coordinated spectra with error bars are plotted in the Supplemental Material.

5. Cluster connectivity

The local structures of the triangular planes of 3-coordinated O atoms and the polyhedral of their neighbor Si atoms at 110 GPa are depicted in Figs. 12(a) and 12(b). According to Ref. [15], Lee *et al.* suggested that the densification of amorphous SiO_2 is achieved by forming O quadclusters above 100 GPa at the expense of 3-coordinated O and 6-coordinated Si atoms. The authors further suggest that the 4-coordinated O atom is corner shared with four Si-$O_{6,7}$ clusters. However, investigations of the structure at 110 GPa show that the densification of amorphous SiO_2 can be described with a different mechanism. As it is shown in Fig. 12(a), the 3-coordinated O atoms, O28 and O47, form triangular planes with three Si atoms, respectively. The two O-Si_3 planes are edge shared with each other. Another 3-coordinated O atom, O6 (not showing the third-neighbor Si atom in this figure), also forms similar edge-shared triangular planes with O28. From the perspective of Si in Fig. 12(b), the Si atoms are all 6-coordinated to O. Each Si-O_6 cluster is edge shared with each other by sharing two O atoms, and therefore some "squares" are observed. The squares can be identified from the bond-angle distribution plots in Fig. 15. The major peak at 96° shows the formation and the high population of the edge-sharing polyhedral. A recent study reported that the corner-shared SiO_4 clusters at ambient pressure can transform to a mixture of corner-shared, edge-shared, and even faced-shared octahedra at high pressure [31]. Thus, the edge-shared mechanism is more common at Mbar pressures than forming 4-coordinated corner-shared OSi_4 clusters.

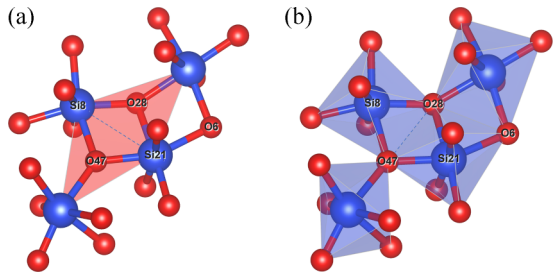

FIG. 12. Illustrations of the edge-shared mechanism from the perspective of O and Si atoms, respectively. (a) Triangular planes of the 3-coordinated O atoms in the amorphous SiO_2 network at 110 GPa. 3-coordinated O atoms are edged shared with each other, i.e., the two triangular planes formed by O47 and O28 share the same edge with Si8 and Si21 as the end points. (b) Polyhedra of neighbor Si atoms to the 3-coordinated O. The polyhedra formed by Si8 and Si21 share the same edge with O28 and O47 as the end points. Similarly, the edge with O6 and O28 as end points is shared by the polyhedron of Si21 and another Si polyhedron on the top right.

6. Electron localization function and bond critical points

The nature of the O-Si "bonding" is analyzed using QTAIM and the electron localization function (ELF). Figure 13 shows the isosurface of the ELF and the bond critical points of the 4-coordinated O clusters found in our FPMD snapshots of amorphous SiO_2 at 198 GPa. The yellow regions are ELF isosurfaces with $\eta = 0.85$. A large value of the ELF is an indication that an "electron-paired bond" is formed between O and Si. For the four configurations shown in Fig. 13, we found that the ELF maxima are located close to three of the BCP along the O-Si axes. In all cases, the fourth ELF maximum is slightly displaced from the BCP of O-Si13 and closer to the oxygen atom. This suggests that it is an oxygen lone pair rather than a genuine O-Si bond. Further analysis reveals that Si13 deviates from the tetrahedral structure. Within a simulation duration of about 1.4 ps, the Si3-O5-Si13 bond angle is around 91°, the Si17-O5-Si13 bond angle is around 96°, and the Si22-O5-Si13 bond angle varies between 119° and 135°. The bond length of O-Si3,

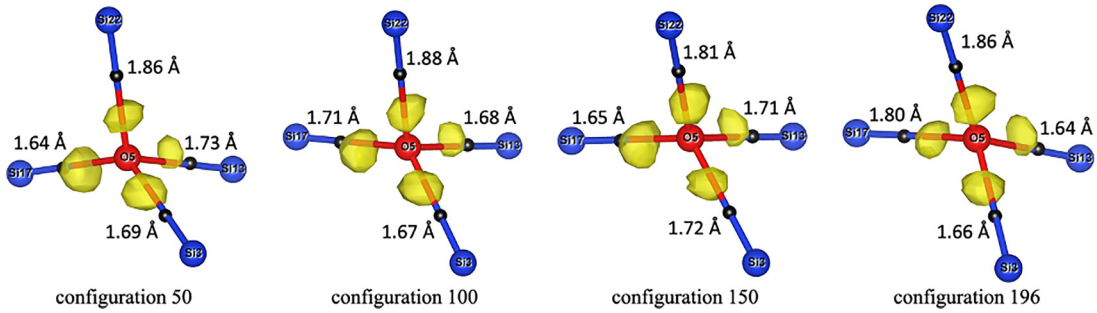

FIG. 13. The ELF and bond critical points of the 4-coordinated O-Si_4 cluster at 198 GPa. The four figures show the same O-Si_4 cluster at different MD configurations. The ELF isosurface is $\eta = 0.85$. The black dots denote the bond critical bonds of O-Si. The time step between each configuration is 7.257 fs, and each figure has a time interval of about 0.362 ps. The total simulation period is 1.422 ps. The cutoff radius is 1.9 Å (Si atoms in blue, and O atoms in red).

O-Si13, O-Si17, and O-Si22 are within the reasonable range from 1.64 to 1.88 Å. However, we can notice that in the O-Si_4 clusters, there are always three shorter O-Si bonds of 1.64 to 1.73 Å, and the other O-Si has a longer distance of over 1.80 Å. As it is shown in Figs. 13(a) to 13(c), the O atom has a longer distance to Si22 of about 1.85 Å. In Fig. 13(d), the distance between O and Si13 is shortened to 1.64 Å, and the O-Si17 distance is increased to 1.80 Å. It indicates that the O in the O-Si_4 structure is fluctuating and there is always one longer O-Si distance, which is outside of the range of a normal O-Si bond (1.65 Å). This agrees with the experimental and FPMD results from Ref. [32] that highly distorted OSi_4 structures with one off-centered O at pressures were observed up to 200 GPa, which share a very similar topology to $OSi_3 + Si$.

Valence electron charge density topological analysis is used to further investigate the bonding. The black dots in Fig. 13 are the bond critical points identified. We can observe bond critical points between O and all four Si atoms. According to the definition, bond critical points (BCP) are the saddle points of electron density between two neighbor atoms [33,34]. BCP has maximum electron density in two directions and minimum in the third direction. It does not necessarily mean that the two atoms actually form a real chemical bond as it could be a geometric consequence even if two atoms are far apart. A more definitive assignment of the interaction can be made from combining results from ELF analysis and bond critical points analysis. Since the ELF gives the probability for electron pairing in the region of space where a bond is more likely to be formed. If the location of the bond critical points coincides with the ELF maximum, it is an unambiguous signature of a genuine chemical bond. Such comparisons are depicted in Fig. 13, where positions of the bond critical points and the distance to the ELF maxima of a O-Si_4 cluster are illustrated. Table I summarizes the estimated relevant distances from the central O atom to the surrounding 4 Si for the four quadclusters at 198 GPa. R_1 is the distance from the central O to the maximum of the ELF and R_2 is the difference in the distance of the BCP and the ELF maximum. In all cases, we found three short R_2 indicating the BCP is closer to the ELF maximum and a longer R_2 where the ELF maximum is further away from the BCP. Another important indicator is the electron density at the bond critical bond. Table II lists the distances d, electron density ρ, potential energy density V, kinetic energy density G, and total energy density H of O-Si of the different configurations at 198 GPa. The total energy densities H are all negative, indicating that the bonds are covalent. At each configuration, the three shorter O-Si bonds have a comparably higher electron density at the bond critical points of values higher than $0.105\, ea_0^{-3}$, where a_0 is the Bohr radius. In comparison, the long bond, O-Si22, has a smaller electron density at the bond critical point of less than $0.1\, ea_0^{-3}$. It shows that a strong O-Si bond is less likely to be formed between O and Si22. Therefore, the four O-Si interactions are not equivalent in the "quadcluster" and it is more appropriate to be described as a "3+1" cluster.

IV. CONCLUSION

We have investigated the possibility of the existence of 4-coordinated O-Si in amorphous SiO_2 glass under high pressure via the calculation of XRS spectra and analysis of the electronic structures based on simulation snapshots from first-principles molecular dynamics calculations. The O-Si RDF at different pressures shows the O-Si distances do not change

TABLE I. Estimates of the distance of the ELF maximum and the BCP along the O-Si direction (R_1) and the difference in the distance of the BCP and the ELF maximum (R_2) of quadclusters in amorphous SiO_2 at 198 GPa. All distances are in Å.

	O-Si3		O-Si13		O-Si7		O-Si22	
	R_1	R_2	R_1	R_2	R_1	R_2	R_1	R_2
Configuration 50	0.64	0.36	0.68	0.34	0.71	0.26	0.61	0.50
Configuration 100	0.64	0.35	0.71	0.27	0.68	0.33	0.60	0.54
Configuration 150	0.65	0.37	0.70	0.32	0.71	0.26	0.62	0.47
Configuration 196	0.64	0.33	0.66	0.30	0.63	0.46	0.59	0.53

TABLE II. Topological properties of O-Si at different configurations at 198 GPa. The O-Si distance is denoted by d, and ρ is the electron density at the BCP. V, G, and H are the potential energy density, kinetic energy density, and total energy density, respectively.

Atoms	d (Å)	$\rho\left(ea_0^{-3}\right)$	V (E_h)	G (E_h)	H (E_h)
Configuration 50					
O-Si3	1.69	0.152	−0.325	0.279	−0.047
O-Si13	1.73	0.131	−0.218	0.144	−0.074
O-Si17	1.64	0.124	−0.253	0.240	−0.013
O-Si22	1.86	0.086	−0.116	0.088	−0.028
Configuration 100					
O-Si3	1.67	0.140	−0.315	0.305	−0.010
O-Si13	1.68	0.133	−0.248	0.196	−0.052
O-Si17	1.71	0.132	−0.251	0.209	−0.042
O-Si22	1.88	0.083	−0.109	0.083	−0.027
Configuration 150					
O-Si3	1.72	0.149	−0.350	0.335	−0.015
O-Si13	1.71	0.128	−0.157	0.034	−0.123
O-Si17	1.65	0.119	−0.211	0.176	−0.035
O-Si22	1.81	0.098	−0.163	0.147	−0.016
Configuration 196					
O-Si3	1.66	0.149	−0.331	0.331	−0.015
O-Si13	1.64	0.141	−0.302	0.274	−0.029
O-Si17	1.80	0.105	−0.169	0.138	−0.031
O-Si22	1.86	0.085	−0.130	0.118	−0.012

noticeably upon compression from 110 to 142 GPa. The lack of variation in the O-Si distances is due to the close pack of the Si and O atoms and stiff covalent bond. However, at higher pressures, the O-Si distances are shortened. This is due to the onset of the 7-coordinated Si-O (Fig. 1). O K-edge XRS spectra at low and high q were calculated. Onsets of the spectra are found to gradually increase in energy with pressure in accordance with experiment. The 2-, 3-, and 4-coordinated components of the XRS spectra were carefully compared. The 2- and 3-coordinated components can be distinguished clearly, while no distinct feature can be attributed to the 4-coordinated O. We showed that the spectrum of 4-coordinated O is very similar to the 3-coordinated O spectrum. Therefore, there are no unique spectral features characterizing the 4-coordinated O. Investigation of the local structure shows that even though the local structure is 4-coordinated, there are always three O-Si distances of about 1.65 Å and one O-Si separation longer than 1.9 Å. Topological analysis of the electron density questions whether the long O-Si can be classified as a "bond." ELF finds isosurfaces along the four O-Si, and QTAIM finds four bond critical points along O-Si. However, the electron density at the BCP is usually one order of magnitude smaller for the long O-Si, compared to the other three BCPs along the short O-Si bonds. The BCP for the long O-Si is also farther away from the ELF isosurface in line with the analysis of the XRS spectra at the oxygen K edge. Therefore, we conclude that O-Si_4 quadclusters do exist, but the fourth O-Si is not a genuine covalent bond. Coordination is not bonding. Coordination simply measures the number of nearest-neighbor atoms. Bonding involves chemical interactions due to the sharing of electrons between two adjacent atoms forming a chemical bond. The theoretical results show the proposed oxygen quadcluster is simply due to a compaction effect and cannot be attributed to the occurrence of new chemical interactions. Moreover, the calculations reproduce the experimental trend we found and no characteristic spectral features can be attributed to the additional oxygen coordination by silicon.

ACKNOWLEDGMENTS

J.S.T. wishes to thank NSERC for a Discovery Grant. We acknowledge the European Synchrotron Radiation Facility (ESRF) for provision of synchrotron radiation and technical support at beamline ID20 as well as computing support and resources.

APPENDIX

1. Radial distribution functions

Figures 14(a) and 14(b) show the O-Si and O-O radial distribution functions in comparison to the radial distribution function (RDF) of SiO_2 glass obtained from the x-ray diffraction experiment shown in Fig. 14(c) [7]. Three peaks observed in Fig. 14(c) can be identified as the Si-O, O-O, and Si-Si separations. In the experiment, a Si-O peak is found at about 1.6 Å at 0 GPa. Upon pressure increase up to 43 GPa, this peak shifts slightly to longer distance of about 1.7 Å. However, with further compression the Si-O shortens to 1.65 Å when the pressure was increased to 172 GPa. The observed trend agrees well with the calculated results. The first O-Si peak shown in Fig. 14(a) is 1.64 Å at 110 GPa. When the pressure is increased to 142 GPa, the position of the first peak does not show any obvious change and as observed in the experiment. At higher pressure, the O-Si distance starts to shorten slightly and the peak shifts to 1.59 Å when compressed to 198 GPa. The shortening simply indicates that the atom arrangement becomes more compact due to the high compression. The first minimum of the O-Si radial distribution function (RDF) is at 2.2 Å. Above 182 GPa, the distribution becomes asymmetric towards the longer distance side (indicated by black arrows). This suggests that more Si atoms are being compressed into the first coordination sphere of the O. In other words, the O atom now has more Si neighbor atoms, but at relatively longer O-Si distances. The pressure dependence of the second peak in the experiment, the O-O RDF, is also consistent with the MD results. As is shown in Fig. 14(b), the O-O RDF included O-O separated by more than 3 Å, which is beyond the first coordination cell. Compared with the shortest dimension of the cell (5.79 Å at 198 GPa), the size of the box is sufficient for investigating the characteristics of the glass structure. In the experiment [Fig. 14(c)], the O-O peak first elongates from 2.5 Å at 0 GPa to 2.6 Å at 14 GPa, then it shortens again to 2.5 Å at 57 GPa. The first peak from FPMD calculations shown in Fig. 14(b) is at 2.28 Å at 110 GPa and shifts to 2.19 Å at 198 GPa. The Si-O RDF shows that compressing amorphous SiO_2 results in the shortening of the average O-Si distance eventually and the O atoms are compacted, thus reducing the volume. However, as discussed in the main text, these changes have no substantial influence on the change in the O-Si coordination.

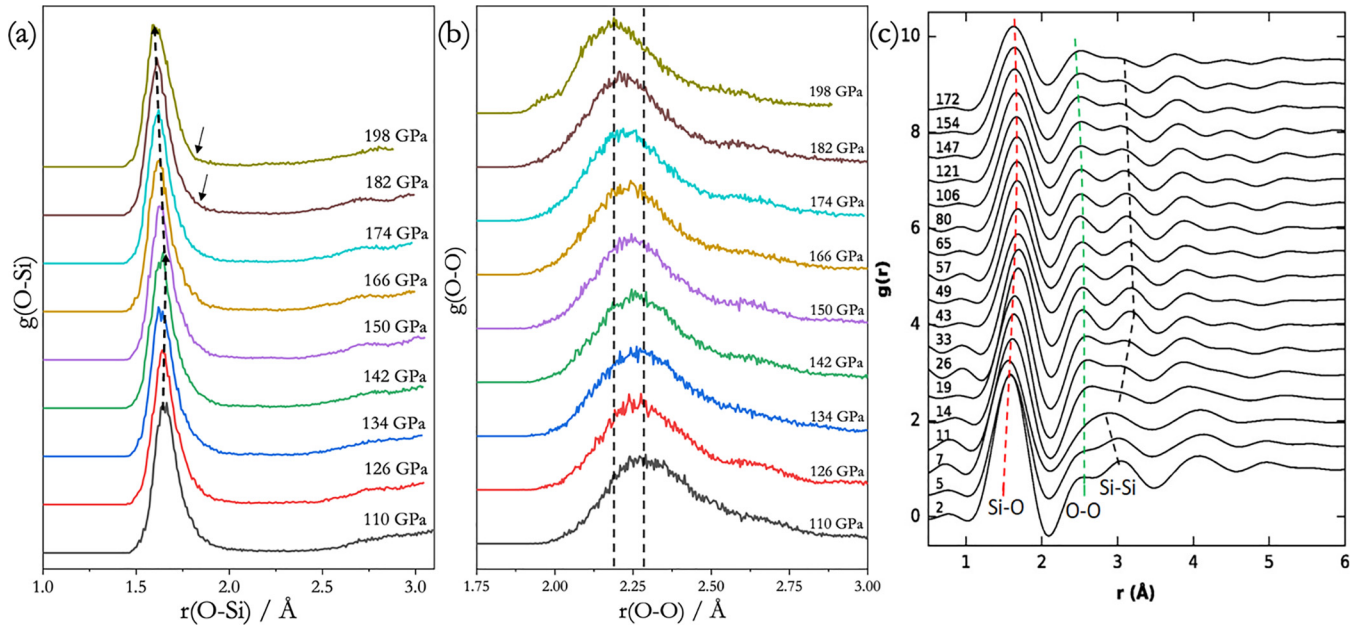

FIG. 14. The radial distribution function of (a) O-Si and (b) O-O extracted from the FPMD simulations of amorphous SiO_2 from 110 to 198 GPa. (c) The RDF of amorphous SiO_2 from the experiment [7].

2. Distribution of bond angles

Figure 15 shows the distribution of O-Si-O and Si-O-Si bond angles at different pressures in Figs. 15(a) and 15(b), respectively. Over the pressure range from 110 to 198 GPa, the distribution of O-Si-O bond angle has a peak at about 82° and a broad band structure at about 165°. We already know from Fig. 1(b) that 6-coordinated Si is dominant in this pressure range, and the fraction keeps increasing with pressure. In 6-coordinated Si octahedra, the Si-O bonds are nearly perpendicular. This leads to a distribution peaked at about 82°. The distribution at 165° is also due to the 6-coordinated Si as two Si-O bonds are along the opposite directions. Due to local

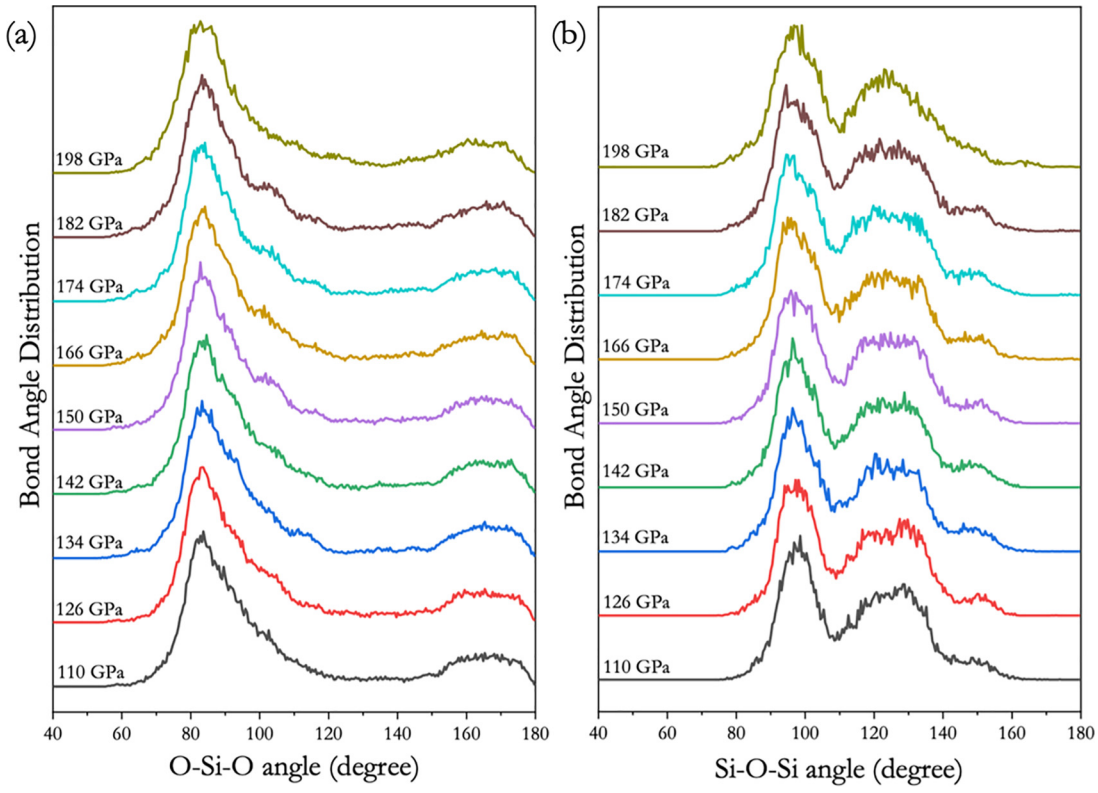

FIG. 15. Bond angle distribution of O-Si-O and Si-O-Si bonds at different pressures.

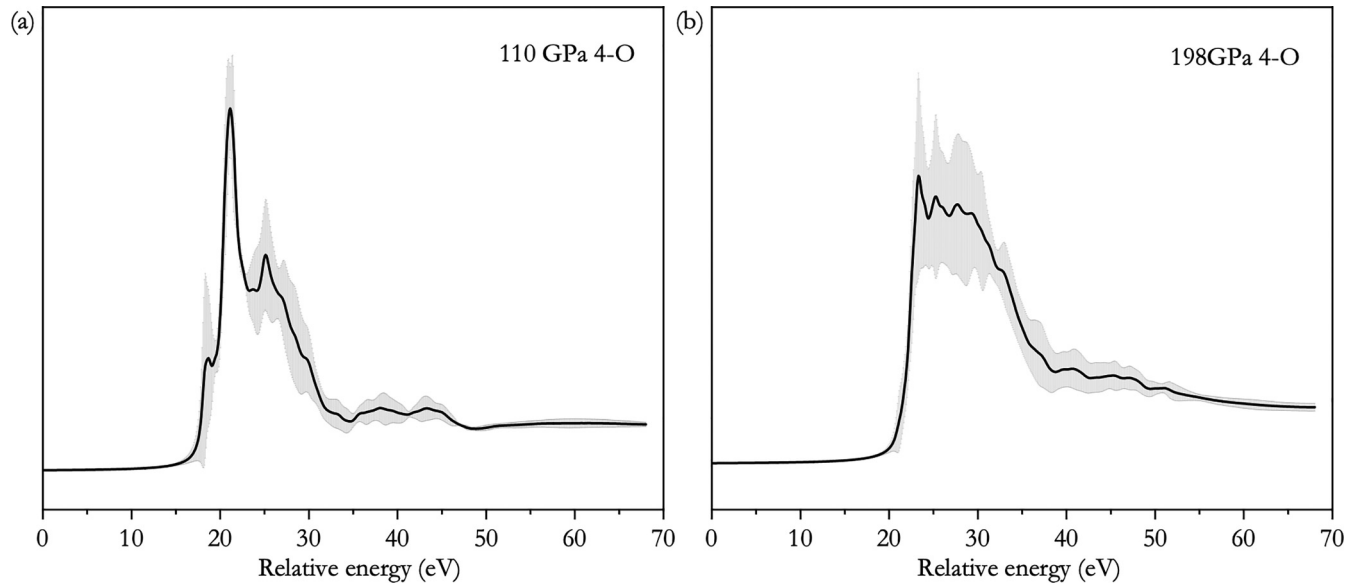

FIG. 16. 4-coordinated O *K*-edge XRS spectra with error bars at low q at 110 and 198 GPa. The cutoff radius is 2.2 Å.

distortion at the Si, the distribution of O-Si-O bond angle deviates from 180°. The distribution also becomes broader with increasing pressure. This is due to a more diverse local environment at high pressure with the appearance of 7-coordinated Si and more distorted 6-coordinated Si-O_6 octahedra. This also results in a slight decrease of O-Si-O at 100°. On the Si-O-Si bond angle distribution, two major peaks are observed at 96° and 124°. The 96° peak reflects the formation of edge-sharing Si-O polyhedra, where two O atoms are shared with each other. The high probability of this peak indicates that many edge-shared "squares" are formed at high pressure. The Si-O-Si bond angles in the square are around 100° and the corresponding O-Si-O bond angles are smaller than 80°. Sometimes two squares are linked together by edge sharing a O-Si bond and form a 3-coordinated O. The other Si-O-Si bond angle varies from 90° to 160°. Similar results in the O-Si-O and Si-O-Si bond angle distribution can be found in Ref. [32].

3. 4-coordinated O *K*-edge XRS spectra at low q

Figure 16 shows the error bars on the 4-coordinated O XRS spectra at 110 and 198 GPa. The error bars indicate the variance of the XRS spectra among different 4-coordinated O atoms.

[1] M. Murakami and J. D. Bass, Spectroscopic evidence for ultrahigh-pressure polymorphism in SiO_2 glass, Phys. Rev. Lett. **104**, 025504 (2010).
[2] S. Petitgirard, C. Sahle, C. Weis, K. Gilmore, G. Spiekermann, J. Tse, M. Wilke, C. Cavallari, V. Cerantola, and C. Sternemann, Magma properties at deep earth's conditions from electronic structure of silica, Geochem. Perspect. Lett. **9**, 32 (2019).
[3] B. B. Karki, D. Bhattarai, and L. Stixrude, First-principles simulations of liquid silica: Structural and dynamical behavior at high pressure, Phys. Rev. B **76**, 104205 (2007).
[4] T. Tsuchiya and J. Tsuchiya, Prediction of a hexagonal SiO_2 phase affecting stabilities of $MgSiO_3$ and $CaSiO_3$ at multimegabar pressures, Proc. Natl. Acad. Sci. USA **108**, 1252 (2011).
[5] M. Wu, Y. Liang, J.-Z. Jiang, and J. S. Tse, Structure and properties of dense silica glass, Sci. Rep. **2**, 398 (2012).
[6] X. Du and J. S. Tse, Oxygen packing fraction and the structure of silicon and germanium oxide glasses, J. Phys. Chem. B **121**, 10726 (2017).
[7] C. Prescher, V. B. Prakapenka, J. Stefanski, S. Jahn, L. B. Skinner, and Y. Wang, Beyond sixfold coordinated si in SiO_2 glass at ultrahigh pressures, Proc. Natl. Acad. Sci. USA **114**, 10041 (2017).
[8] S. S. Lobanov, S. Speziale, B. Winkler, V. Milman, K. Refson, and L. Schifferle, Electronic, structural, and mechanical properties of SiO_2 glass at high pressure inferred from its refractive index, Phys. Rev. Lett. **128**, 077403 (2022).
[9] S. Petitgirard, C. J. Sahle, W. J. Malfait, G. Spiekermann, I. Blanchard, E. S. Jennings, M. Cotte, and M. Murakami, Anomalous density, sound velocity, and structure of pressure-induced amorphous quartz, Phys. Rev. B **105**, 134106 (2022).
[10] T. Sato and N. Funamori, High-pressure structural transformation of SiO_2 glass up to 100 GPa, Phys. Rev. B **82**, 184102 (2010).
[11] T. Sato and N. Funamori, Sixfold-coordinated amorphous polymorph of SiO_2 under high pressure, Phys. Rev. Lett. **101**, 255502 (2008).
[12] V. V. Brazhkin, Comment on "sixfold-coordinated amorphous polymorph of SiO_2 under high pressure", Phys. Rev. Lett. **102**, 209603 (2009).
[13] Y. Liang, C. R. Miranda, and S. Scandolo, Mechanical strength and coordination defects in compressed silica glass: Molecular dynamics simulations, Phys. Rev. B **75**, 024205 (2007).
[14] A. Zeidler, K. Wezka, R. F. Rowlands, D. A. J. Whittaker, P. S. Salmon, A. Polidori, J. W. E. Drewitt, S. Klotz, H. E. Fischer, M. C. Wilding, C. L. Bull, M. G. Tucker, and M. Wilson,

High-pressure transformation of SiO_2 glass from a tetrahedral to an octahedral network: A joint approach using neutron diffraction and molecular dynamics, Phys. Rev. Lett. **113**, 135501 (2014).

[15] S. K. Lee, Y.-H. Kim, Y. S. Yi, P. Chow, Y. Xiao, C. Ji, and G. Shen, Oxygen quadclusters in SiO_2 glass above megabar pressures up to 160 GPa revealed by x-ray raman scattering, Phys. Rev. Lett. **123**, 235701 (2019).

[16] J. Vinson, J. J. Rehr, J. J. Kas, and E. L. Shirley, Bethe-salpeter equation calculations of core excitation spectra, Phys. Rev. B **83**, 115106 (2011).

[17] K. Gilmore, J. Vinson, E. L. Shirley, D. Prendergast, C. D. Pemmaraju, J. J. Kas, F. D. Vila, and J. J. Rehr, Efficient implementation of core-excitation bethe–salpeter equation calculations, Comput. Phys. Commun. **197**, 109 (2015).

[18] P. Giannozzi, S. Baroni, N. Bonini, M. Calandra, R. Car, C. Cavazzoni, D. Ceresoli, G. L. Chiarotti, M. Cococcioni, I. Dabo *et al.*, Quantum espresso: a modular and open-source software project for quantum simulations of materials, J. Phys.: Condens. Matter **21**, 395502 (2009).

[19] QUANTUM ESPRESSO is a community project for high-quality quantum-simulation software, based on density-functional theory, and coordinated by Paolo Giannozzi.

[20] E. E. Salpeter and H. A. Bethe, A relativistic equation for bound-state problems, Phys. Rev. **84**, 1232 (1951).

[21] A. Otero-de-la-Roza, M. Blanco, A. M. Pendás, and V. Luaña, Critic: a new program for the topological analysis of solid-state electron densities, Comput. Phys. Commun. **180**, 157 (2009).

[22] A. Otero-de-la-Roza, E. R. Johnson, and V. Luaña, CRITIC2: A program for real-space analysis of quantum chemical interactions in solids, Comput. Phys. Commun. **185**, 1007 (2014).

[23] R. Bader, *Atoms in Molecules: A Quantum Theory* (Oxford University Press, New York, 1990).

[24] R. F. Bader, Atoms in molecules, Acc. Chem. Res. **18**, 9 (1985).

[25] R. F. Bader, A quantum theory of molecular structure and its applications, Chem. Rev. **91**, 893 (1991).

[26] R. F. Bader, The quantum mechanical basis of conceptual chemistry, Chem. Monthly **136**, 819 (2005).

[27] See Supplemental Material at http://link.aps.org/supplemental/10.1103/PhysRevB.109.054110 for the radial distribution function of O-Si and O-O; the O-Si-O and Si-O-Si bond angle distribution; 4-coordinated O K-edge XRS spectra with error bars at 110 and 198 GPa. The Supplemental Material also includes Refs. [7] and [32].

[28] P. Chow, Y. Xiao, E. Rod, L. Bai, G. Shen, S. Sinogeikin, N. Gao, Y. Ding, and H.-K. Mao, Focusing polycapillary to reduce parasitic scattering for inelastic x-ray measurements at high pressure, Rev. Sci. Instrum. **86**, 072203 (2015).

[29] C. J. Sahle, A. Rosa, M. Rossi, V. Cerantola, G. Spiekermann, S. Petitgirard, J. Jacobs, S. Huotari, M. Moretti Sala, and A. Mirone, Direct tomography imaging for inelastic x-ray scattering experiments at high pressure, J. Synchrotron Radiat. **24**, 269 (2017).

[30] J. Stöhr, *NEXAFS Spectroscopy* (Springer, New York, 2013), Vol. 25.

[31] A. Hasmy, S. Ispas, and B. Hehlen, Percolation transitions in compressed SiO_2 glasses, Nature (London) **599**, 62 (2021).

[32] M. Murakami, S. Kohara, N. Kitamura, J. Akola, H. Inoue, A. Hirata, Y. Hiraoka, Y. Onodera, I. Obayashi, J. Kalikka *et al.*, Ultrahigh-pressure form of SiO_2 glass with dense pyrite-type crystalline homology, Phys. Rev. B **99**, 045153 (2019).

[33] R. F. Bader and H. Essén, The characterization of atomic interactions, J. Chem. Phys. **80**, 1943 (1984).

[34] S. Shahbazian, Why bond critical points are not "bond" critical points, Chem. Eur. J. **24**, 5401 (2018).